Drop-Casted Self-Assembling Graphene Oxide Membranes for Scanning Electron Microscopy on Wet and Dense Gaseous Samples

Mark Krueger,[†] Shannon Berg,[†] D'Arcy Stone,[†] Evgheni Strelcov,[†] Dmitriy A. Dikin,[‡] Jaemyung Kim,[‡] Laura J. Cote,[‡] Jiaxing Huang,[‡] and Andrei Kolmakov[†,*]

[†]Department of Physics, Southern Illinois University, Carbondale, Illinois 62901, United States and, [‡]Northwestern University, Evanston, Illinois 60208, United States

ABSTRACT

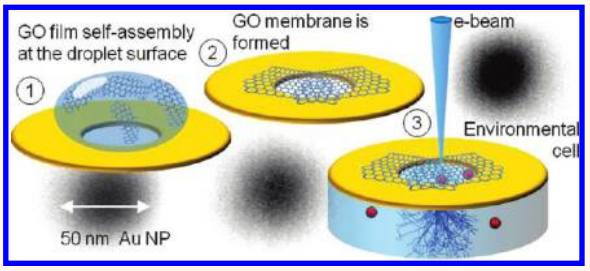

Graphene oxide sheets dispersed in water and many other solvents can spontaneously assemble into a surface film covering an evaporating droplet due to their amphiphilicity. Thus, graphene oxide membranes with controllable thickness suspended over an orifice have been directly fabricated using a simple drop-cast approach. Mechanical properties and electron transparency tests of these membranes show their use as electron transparent, but molecularly impenetrable, windows for environmental electron microscopy in liquids and dense gaseous media. The foreseeable, broader application of this drop-cast window methodology is the creation of access spots for electron probes to study isolated microsamples in their natural, undisrupted state within the interior of prefabricated devices (such as microfluidic chips or sealed containers of biological, chemically reactive, toxic, or forensic materials).

KEYWORDS: graphene oxide · *in situ* electron microscopy · self-assembled membrane · drop-casting

The current needs of material, biological, medical, and catalytic research to image objects and dynamic processes in their native environment constitutes the driving force in the developments of high-resolution *in situ/in vivo* microscopy of objects immersed in dense gaseous and liquid environments at pressures above 10−100 Torr. Electron microscopy has a long history in the development of both closed and differentially pumped environmental cell (E-cells) designs.[1−8] The variety of applications of electron microscopy in dense media has been demonstrated during recent years,[9−13] and a few commercial E-cells for electron microscopy of dense media are currently available.[14]

The design of closed E-cells for electron microscopy crucially depends on the electron transparency and mechanical stability of the pressurized membrane windows. As a compromise between these two major requirements, the typical windows made of SiO_2, SiN, or polyimide membranes have a thickness of 50−150 nm and a working area ranging from a few to a few hundred square micrometers. To improve image quality further and work with lower electrons energies, thinner membranes made of lower Z materials would be preferable.

Lately, high-yield protocols to fabricate suspended membranes made of graphene (G) or a graphene derivative, such as graphene oxide (GO), have been proposed.[15−22] Due to graphene and its derivatives' high electron transparency,[23,24] high thermal/electrical conductivity, monolayer thickness, inherently high breaking strength,[25−29] and gas/liquid impermeability,[25,27] they represent a nearly ideal choice of membrane material for environmental cells.[30] The Langmuir−Blodgett (LB) deposition technique has been used, which is suitable for the fabrication of very thin (one or a few monolayers thick) GO membrane windows. In the LB deposition,[31] the GO sheets were directly spread onto the water surface without any modification due to their amphiphilicity. In addition, recent works have revealed that GO sheets can be enriched at the air−water interface through flotation, can stabilize emulsions of organic solvents and can act as surfactant to disperse insoluble materials (such as graphite and carbon nanotubes).[32,33] Therefore, drying a droplet of GO containing

* Address correspondence to akolmakov@physics.siu.edu.

Received for review October 10, 2011 and accepted November 21, 2011.

Published online November 21, 2011
10.1021/nn204287g

dispersion can lead to the formation of a thin membrane coating the surface.[32]

In this communication, we demonstrate a simple drop-casting protocol to fabricate free-standing GO membranes with thicknesses ranging from a few to a few hundred nanometers created directly over a small orifice (5−50 μm in diameter) by taking advantage of GO's high surface activity. As a proof of concept for their use by scanning electron microscopy under wet conditions, the electron transparency and mechanical stability of these spontaneously formed membranes were tested using 50 nm Au nanoparticles suspended in water as a model sample. This method of creating GO membranes does not require any sophisticated microfabrication protocol, thus it can be conveniently used for fabrication of electron transparent windows in pre-existing devices, (micro-) chambers and vessels. It is necessary to note that recent reports on the atomic structure of GO and partially reduced GO revealed that some nanometer size holes could be found in the individual sheets.[34,35] However, with at least a few layers of randomly overlapping GO sheets, molecular permeability through the windows can be drastically reduced. Although fabricating of such windows from more perfect graphene should improve membrane impermeability, the use of solution-processable GO is facile and much more versatile.

We tested different commercial apertures (see Methods section) as supporting frames for the GO windows without any noticeable difference in behavior or characteristics of the membranes. Depending on the ratio between the microhole diameter *d* and the thickness *h* of the orifice, two protocols were tested to fabricate GO electron transparent windows (Figure 1). In the case of small (4−10 μm) apertures, two droplets (one of GO aqueous solution and the other of pure water) were placed to opposite sides of the metal frame (Figure 1b) using a calibrated micropipet. The droplet of pure water was *ca.* 10 times larger compared to a *ca.* 2−3 μL droplet containing GO. Due to the amphiphilicity of GO sheets,[32] the latter, being initially homogeneously distributed in the bulk of smaller droplet, become segregated at the water−air interface of the smaller droplet (Figure 1c)[33,36] and the GO membrane self-assembles at the water−air interface. This rudimentary and loosely packed GO membrane at the interface is partially water vapor permeable at this stage due to incomplete coverage of the GO sheets. As a result, the droplet evaporates slowly (Figure 1d), resulting in gradual densification of the interfacial GO membrane. The role of the large, water backing droplet is to serve as a gentle supporting media for the GO membrane while drying occurs. Prior to complete evaporation of the backing droplet, the water was slowly substituted with acetone to minimize the surface tension coefficient, thus avoiding capillary-induced collapse of the membrane

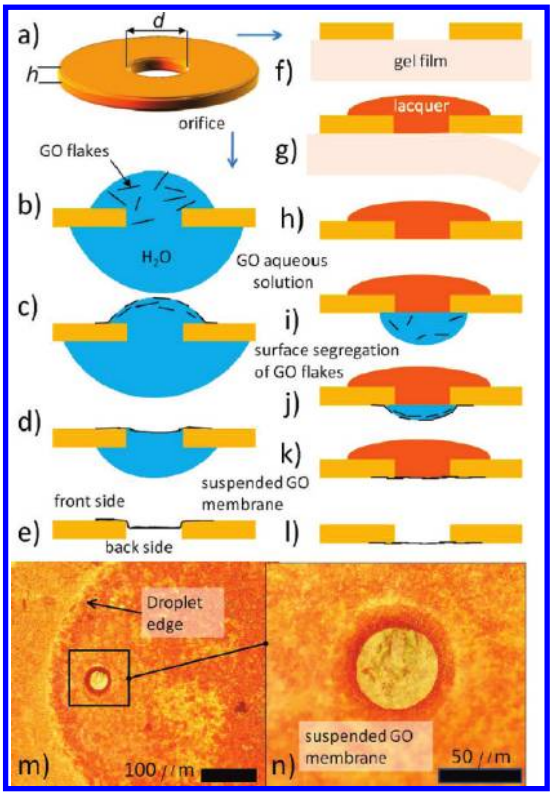

Figure 1. Two protocols for drop-cast fabrication of the GO membranes. Left panels (a−e) have been used to prepare membranes over few micrometer size apertures; the protocol in the right panels (f−l) can be used for larger orifices few tens of micrometers wide; (m,n) optical images of the GO membrane prepared on the copper orifice.

during the latter stages of drying (see Methods section). Since this method does not involve any additional chemical treatment, the resultant membrane has the ultimate purity attainable, thus reducing the propensity of the few micrometer aperture from being clogged by any processing residues.

The second method is designed for the deposition of a GO membrane on one side of the large (10−50 μm) apertures (Figure 1f−l). The detailed protocol is described in the Methods section. Briefly, the orifice was filled with the polymer to create the smooth surface coplanar with the front of the frame (Figure 1f−h). The droplet of GO aqueous solution was placed over the filled orifice (Figure 1i), and similar to the previous case, the GO membrane was formed upon the slow drying of the droplet (Figure 1j,k). The polymer support was slowly dissolved in acetone to create a free-standing GO membrane (Figure 1l). After the preparations, all membranes were subsequently dried at 125 ± 5 °C in air for half an hour. This procedure eliminates the excess of interlayered water, strengthens the membrane, and improves its adhesion to the frame surface.[28]

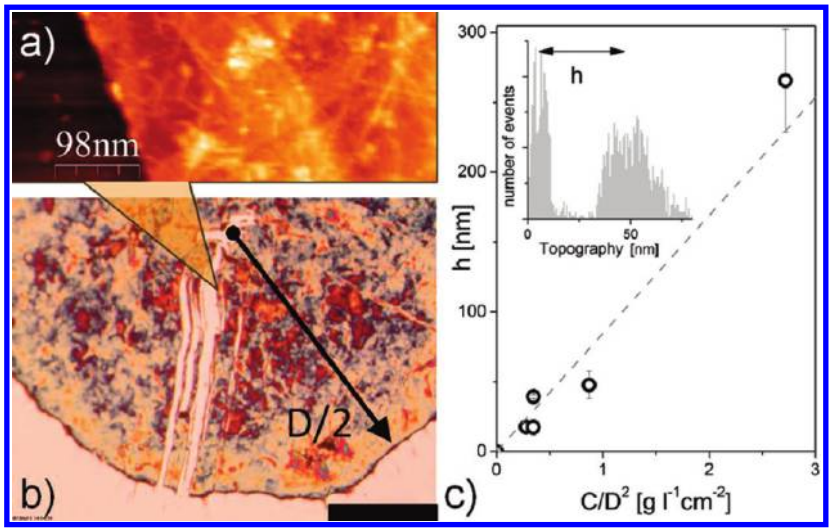

Figure 2. (a) AFM image of the membrane edge; (b) optical image in polarized light of the dried GO solution. The scratched area was used to define the thickness of the membrane. The scale bar corresponds to 250 μm; (c) step height histogram measured using AFM at the ridge of the scratch.

RESULTS AND DISCUSSION

Membrane Characterization. Different from standard SiO_2 or SiN membrane microfabricaton technologies, the drop-cast method offers the opportunity to create the membranes selectively at predefined location and with adjustable thicknesses. For both protocols, the thickness h of the membrane can be controlled *via* dilution level C_{GO} of the primary GO solution and/or the diameter D of the contact area of the droplet using the simple relation $h = (4V_L/\pi\rho_{GO})(C_{GO}/D^2)$, where V_L and ρ_{GO} are the initial volume of the droplet and the density of the solid GO membrane, correspondingly. Since the droplet contact line remains pinned during the drying process, the thickness can be easily controlled in the range from few to hundreds of nanometers (see below). The typical diameter of the contact area of the droplet on Si/SiO_2 wafers and on metal apertures was on the order of 1 mm under normal conditions and can be tuned by (i) modifying the wetting properties of the substrate or (ii) creating a hydrophobic barrier of a predefined diameter using a liquid blocker (EM Sciences). To examine this dependence, an array of equivalent 3 μL droplets with different concentrations of GO was allowed to dry on the clean Si/SiO_2 surface. After drying, part of the residual GO film was mechanically removed along the radius and step height histograms were measured using AFM at different locations along the ridge (Figure 2a,b). Figure 2c depicts the experimentally obtained average height values as a function of the GO dilution level C_{GO} and drop contact diameter D. Nearly linear dependence confirms that the film thickness is rather homogeneous along the diameter and no appreciable coffee-ring effect was observed (Figure 2b).[37] This implies that for such droplets the irreversible surface segregation rate of GO sheets to the interface is significantly larger compared to the droplet evaporation time.

Morphology and Mechanics of the Suspended Membranes. A special cell having a gas inlet and connection to a highly accurate pressure gauge was designed to facilitate monitoring of the morphological changes and deflections of the membrane during pressurization. The typical topology of the 40 nm thick membrane suspended over 50 μm orifice is depicted in Figure 1m,n and at higher magnification in Figure 3. The rippled surface of the dry membrane is due to the fact that GO membranes are usually formed on the concaved/convex surface of the droplet depending on its drying history (Figure 1c,d). In addition, different expansion coefficients and slipping of the GO film on the support surface during the annealing and cooling cycle can also contribute to the observed corrugations. The formation of concave/convex membranes can lead to "flip-flopping" behavior upon pumping (Figure 3a). For suspended membranes as large as 50 μm in diameter, the height variations between "valleys" and "hills" can reach a few micrometers, which hinders roughness analysis using AFM. Optical profilometry (Nanovea) was employed instead for quantitative analysis of the membrane morphology and mechanics during pressurization (Figure 3b,c). With a pressure differential, most of the initial slack of the membrane can be removed, and flattening usually takes place at $\Delta P < 10^4$ Pa. Further increase of the pressure leads to the development of the tensile strain in the membrane and finally its disruption (not shown here). More than 30 membranes with the thicknesses between 20 and 250 nm and orifice diameters between 4 and 50 μm have been tested. For large fields of view, the 50 μm membranes with the thickness of *ca.* 30−50 nm were found to be the best practical compromise between

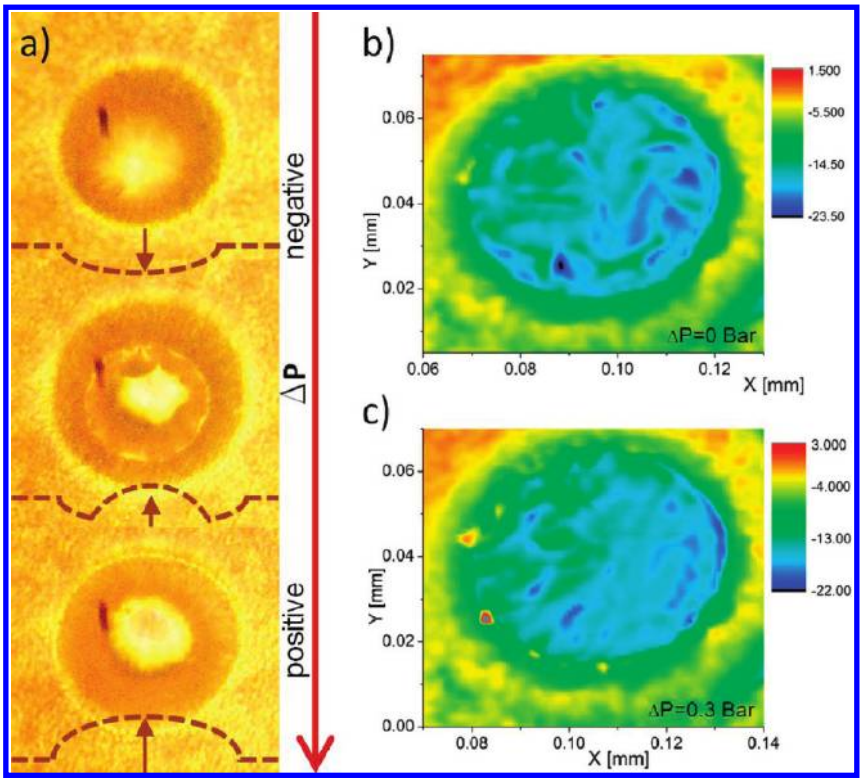

Figure 3. (a) Optical image of the 50 μm membrane showing flip-flopping behavior during the pressurizing cycle; (b) topography of the released and pressurized membrane measured quantitatively using optical profilometry. The color scheme corresponds to high variations measured in micrometers.

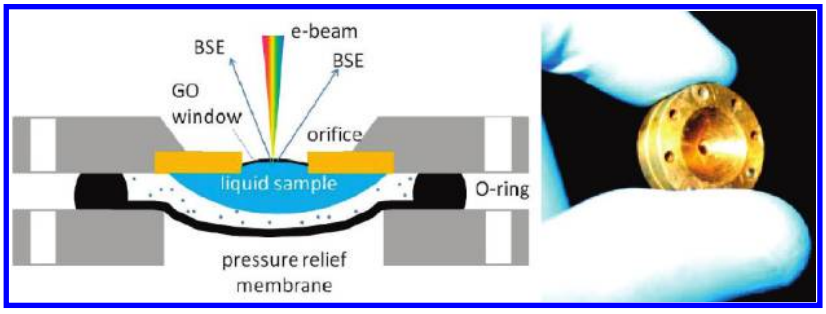

Figure 4. Principle design (left) and characteristic dimensions of the E-cell (right panel).

requirements of the mechanical stability and electron transparency. These membranes were capable of withstanding the pressure differential up to 1.3×10^5 Pa, which is sufficient for most practical needs of environmental electron microscopy. Smaller membranes (<10 μm in diameter) can withstand a similar pressure differential even if they are as thin as a few nanometers. Using the bulge test method,[38] the tensile strength σ_{max} of circular GO membranes can be evaluated.[39] Measuring the bulge height h (after the removal of the initial slack) and P_{max} of the pressurized suspended membrane, along with the thickness t and diameter D just before the failure for typical 40 nm thick and 50 μm wide membranes, the average stress $\sigma_{max} = (P_{max} \times D^2)/(16ht)$ was evaluated to be ~80 MPa, which is close, but somewhat lower compared to the reported ~120 MPa tensile strength value for GO paper.[28]

E-Cell Design and Sample Requirements. Figure 4 shows one of the tested designs of the E-cell. The cell is made of two metal discs and is sealed with a pressure relief rubber membrane gasket. The latter serves to isolate the *ca.* 20 μL compartment and to eliminate an overpressure onto the GO membrane when the sample (liquid) contains an excess of trapped gas. This approach was invented by Quantomix Inc.,[40] and it drastically simplifies the cell design and improves its reliability. Such cell is capable of preserving an interior wet environment for months. The interfacial water diffusion between the GO membrane and supporting frame was found to be one of the possible channels for vacuum leaking especially in the cases when the membrane is pressurized from the back side (Figure 1e). This can be significantly reduced *via* simply flipping the supporting frame and using

the GO covered plane as the cell's interior surface (Figure 1i).

The crucial requirement for SEM imaging with membrane-based E-cells is the proximity of the sample to the backside of the membrane.[8,13] The liquid containing samples (such as nanoparticle (NP) solutions) can be drop-casted directly onto the backside of the GO membrane. The adhered nanoparticles become immobilized at the backside of the membrane and therefore can easily be imaged. However, free nanoparticles in Brownian motion usually move too fast compared to the beam rastering rate. The placement of nonplanar or large rigid samples that do not adhere to the membrane surface cannot be realized simply by pressing them mechanically against the membrane due to its probable disruption. To overcome this impediment, we have developed an encapsulation methodology, which employs the secondary drop-casted GO membranes as a capping agent (unpublished data). Using this encapsulation method, potentially any sample can be gently adhered to the surface of the electron transparent membrane while the wet environment around the sample can be preserved.

SEM Imaging. Figure 5a,b represents the typical SEM images of the closed wet cells equipped with 10 μm GO window and filled with the Au NP solution. Panels a and b of Figure 5 were obtained under the same conditions using a back-scattered electron detector (BSED) and an Everhart–Thornley detector (ETD), respectively. Since the ETD is sensitive to low-energy secondary electrons, greater detail of the membrane surface morphology (such as multiple GO wrinkles) can be seen. The profile analysis (Figure 5c) of the individual 50 nm Au nanoparticles revealed that a 20–40 nm thick GO membrane does not deteriorate the resolution of the microscope for the objects attached to or in close proximity (0–50 nm) to the back side of the membrane. Figure 5d demonstrates that EDX analysis can routinely be performed on the objects immersed in the water. However, probing the interior of the few micrometers orifices (which were tilted 39°) leads to a significant contribution of background X-rays from the surrounding stainless steel frame to that of the total EDX spectrum. An accurate protocol for qualitative EDX analysis for such samples has yet to be developed.

The detailed analysis of images taken with the ET detector as a function of the beam energy reveals particularities of the contrast formation mechanism. Namely, it was possible to image Au NPs through the GO membrane using unprecedentedly low electron beam energies (starting form 2 keV). Since the thickness of the membrane (20–40 nm) significantly exceeds the inelastic mean free path for secondary electrons in GO,[30] it is plausible to assume that the SEM signal from Au NPs is formed mainly by secondary electrons of type S_{II} and S_{III} induced by electrons backscattered from the Au NP.[42] For qualitative evaluation

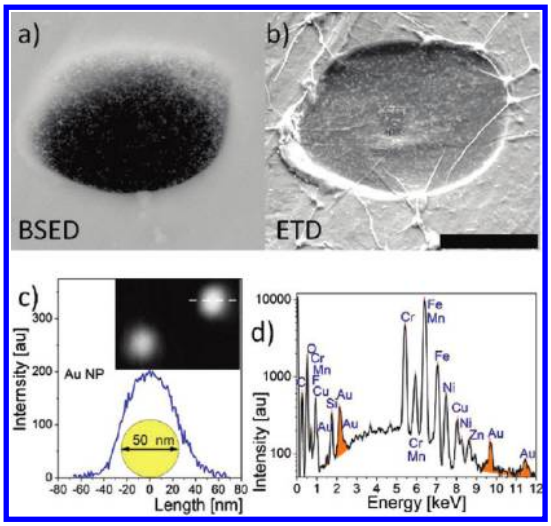

Figure 5. (a) SEM image of the Au NP solution taken in BSE through *ca.* 40 nm GO membrane. Image conditions: 30 keV, tilt 39°; (b) SEM taken under the same conditions but using a surface-sensitive Everhart–Thornley detector. The scale bar corresponds to 5 μm. (c) Line profile over the individual 50 nm Au nanoparticle immersed in liquid water and adhered to the bottom of the membrane. (d) Exemplary EDX spectrum taken from Au NP aqueous solution through the GO membrane. The majority of the unmarked peaks originate from the surrounding stainless steel frame.

of the electron transparency of GO membranes, we used the dependence of the gray scale difference between Au NPs and water ($S_{Au}-S_w/S_{Au}$) as a function of electron beam energy (Figure 6g, black squares). The results were compared with experimental data (triangles and circles in Figure 6g) adopted from refs 8 and 43. It can be noticed that the GO membrane becomes reasonably transparent for electrons already at 2 keV, significantly outperforming the standard commercial ~150 nm polyimide (Quantomix) and 100 nm SiN membranes. The complementing analysis of the apparent nanoparticle density as a function of the beam energy indicates a gradual increase of observable NP with excitation energy. The latter is presumably due to increased range of higher energy electrons, which allows probing through the thicker local patches of the GO membrane and/or deeper into the water.

Finally, we observed interesting phenomenon of electron-beam-induced directional movement of nanoparticles, which were weakly bound to the backside of the membrane. Figure 7a–c represents three sequential scans over the same area of the membrane, which covers the solution of 50 nm Au nanoparticles. While the scans in the Figure 7a,c were recorded at the rastering rate of *ca.* 4×10^5 nm/s, the scan in Figure 7b was recorded at significantly slower rate of *ca.* 3×10^4 nm/s. The appearance of "ghost" traces in Figure 7c is an indication that the Au NPs became mobile during the scan. The effect of relocation of the nanoparticles can be seen by direct comparison of the image Figure 7a and Figure 7c and in the zoomed out image of Figure 7d. This implies that prolonged interaction of

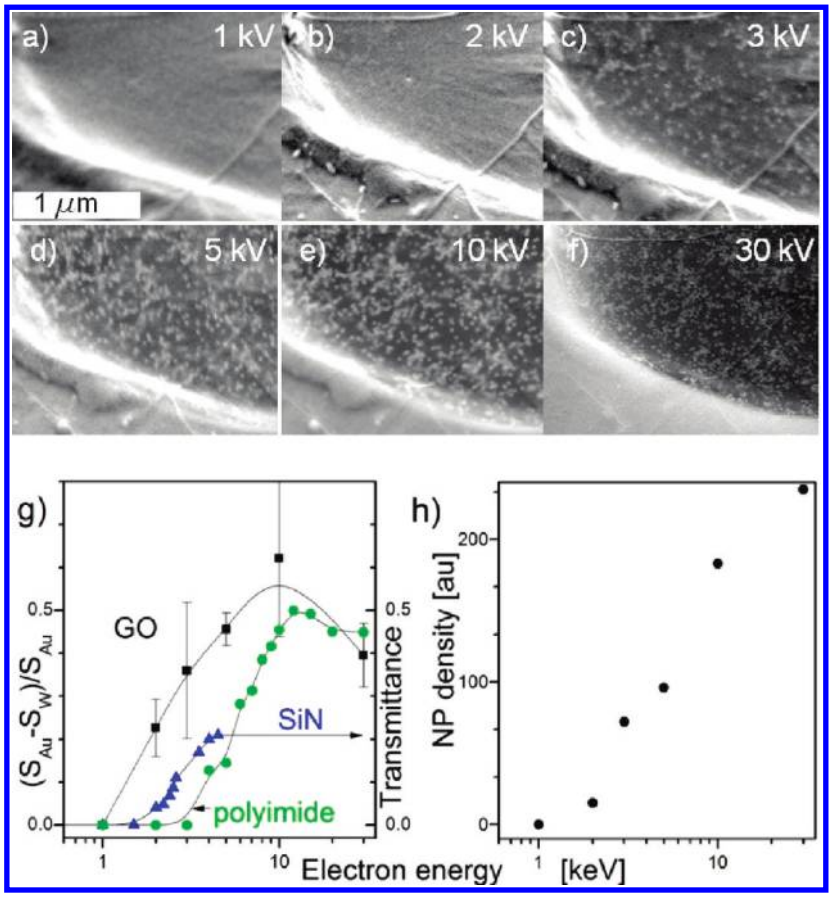

Figure 6. (a–f) Sequential SEM images of the same area of the GO membrane acquired with ET detector as a function of electron beam energy. (g) Relative signal (black squares) from Au NPs a function of electron beam energy. For comparison, the data for commercial 150 nm polyimide (circles) adapted from ref 8 and 100 nm SiN membranes (triangles) adapted from ref 43 are shown; (h) apparent density of Au NPs under GO membrane measured from the same area as a function of electron beam energy.

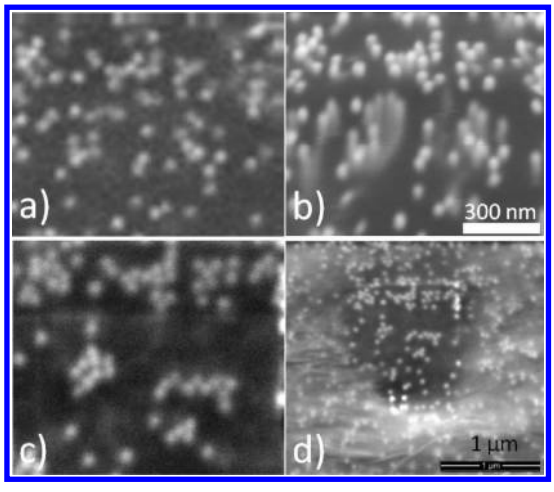

Figure 7. (a,b) Sequential scans over the same area of *ca.* 1 × 1 μm^2, indicating the beam-induced dragging of the weakly adhered Au nanoparticles at lower scanning rate (b). (d) Zoom out image of the scanned area. Partial ordering of the nanoparticles and their accumulation at the borders of the scanning area can be noticed.

the electron beam with a weakly adhered nanoparticle creates a dragging force. The exact nature of this phenomenon requires separate study; however, one can assume that prolonged exposure of the NP to high-energy electrons leads to accumulation of the electrostatic charge in it, which exceeds its dissipation rate into the surrounding media. The latter, in turn, triggers the Coulombic interaction of the NP with the electron beam and/or with the excess of electrons/ions in interaction volume in the surrounding media. As can be seen in the images of Figure 7c,d, this slow rastering leads to some degree of alignment of the nanoparticles along the scanning direction and their accumulation in the right side of the scanning area. This effect of "settling" of randomly distributed nanoparticles into the regular lattice or chain aggregates along with their controllable dragging to specific location by the electron beam can be seen as kind of electron-beam-induced lithography with nanoparticles in liquids and needs to be explored in the future.

We also observed that prolonged exposure of the same GO membrane area to an electron beam with the areal dose in excess of 10 C/cm^2 may lead to darkening of the background (Figure 7d) and some morphological changes of the membrane along its perimeter (Figures 5b and 7d). Similar beam-induced distortions (shrinking) of GO membranes in vacuum were reported

during TEM characterization upon exposure to electrons with doses on the order of 10^3 C/cm^2.[44] While the reported morphological and electronic changes in GO membranes suspended in vacuum can be explained in terms of electron-induced surface and interlayer reduction and defect formation, the case of GO membrane interfacing with liquid water can be more complicated and to the best of our knowledge has not been explored. The observed "improvement" of membrane transparency can be explained by the decrease of the water background signal relative to the one from the nanoparticles. This effect can have two origins: (i) the deposition of an additional carbon layer onto the scanned area due to electron-induced cracking of hydrocarbons from the residual gas and (ii) microbubble formation beneath the membrane. In the former case, these are low-energy secondary electrons from the deeper interfacial water layers, which are primarily attenuated by a newly formed carbon layer. Alternatively, if a microbubble is formed in the irradiated area, the amount of secondary electrons from the water vapor becomes drastically reduced compared to the liquid phase and the nanoparticles that are adhered to the membranes, resulting in darkening of the bubble area in the ET SEM image. In both cases, the tension in the scanned area of the membrane can cause the morphological changes.

CONCLUSIONS AND OUTLOOK

In summary, the solution processability of graphene and graphene derivatives coupled with their high electron transparency and mechanical strength make this class of 2D and quasi-2D window materials a prospective platform for *in situ* environmental electron microscopy. The potential limitation of any membrane-based environmental SEM/TEM imaging technology is damage of the membrane induced by prolonged irradiation from the electron beam. However, experiments show that membrane deterioration only takes place at very large areal doses in excess of 10 C/cm^2 for few kilovolt electrons. In addition, these inexpensive suspended membranes are designed for a single use thanks to well-developed techniques such as spin coating, Langmuir–Blodgett, drop-casting, dip coating, and spraying suitable for large-scale production. The advantage of the drop-cast technique, described in this study, is that the membrane can be realized at an arbitrary location which can be beneficial for creating molecularly impenetrable, yet SEM accessible, areas in pre-existing devices or objects such as microfluidic chips or devices possessing microcracks requiring analysis.

METHODS

Fabrication of the GO Membrane Windows. A GO dispersion in water of 1 mg/mL was obtained using a modification of Hummers method[41] (see details in ref 31). The average lateral size of the GO sheets was on the order of a few to a few tenths of micrometers. We have used electrochemically formed (SPI Supplies) or laser-drilled metal orifice discs made of Cu, Ni, and stainless steel (National Aperture, Inc.) as well as SiN, SiO_2 (SiMPore Inc./TEM windows), and ruby (Bird Precision Inc.) (with diameters from 3 to 9.5 mm and thickness of $h \sim 20$ μm as the frames to support the GO membranes). The orifice diameters ranged from 4 to 50 μm. To fabricate GO windows over the few micrometer holes, we placed *ca.* 20 μL primary drops of distilled water into the array of wettable wells of PTFE printed slides (Electron Microscopy Sciences). UV-ozone-cleaned (Jelight Company Inc.) apertures were placed on top of the primary drop of water, and a small secondary droplet of 1 mg/mL GO solution was drop-casted over the aperture opening. Upon evaporation of the secondary droplet and formation of the GO membrane, the water of the primary droplet was slowly substituted with acetone using a micropipet to relieve the surface tension. Upon complete drying, the orifice with the suspended membrane was annealed in air at 125 $\pm$ 5 °C for half an hour.

To create a temporary mechanical support during the formation of the large membrane, the aperture was placed on the surface of a fresh gel film (Gel-Pak), which tightly and reversibly adheres to the front surface of the aperture. Easily soluble in acetone liquid nail polish (Electron Microscopy Sciences) was drop-casted on to the back side of the aperture (Figure 1g). After drying of the lacquer drop, the gel film was removed leaving the smooth, solid, lacquer surface coplanar with the front of the supporting metal frame (Figure 1h). The front side of the frame was UV-cleaned to improve its hydrophilicity, and a microdroplet of GO solution was placed over the filled hole (Figure 1i). After the droplet had dried and the self-assembly of the GO membrane concluded, the polymer support was dissolved in acetone to release the free-standing membrane. Upon complete drying, the orifice with the suspended membrane was annealed in air at 125 $\pm$ 5 °C for half an hour. After inspection with high-magnification 400×–1000× optical or electron microscope, the orifice was mount inside the environmental cell.

SEM, AFM Imaging. AutoProbe CP-Research AFM (Thermomicroscopes/Veeco) operating in air was used for imaging of the GO deposits on Si/SiO_2 wafers. The probe (resonant frequency 80 Hz) was rastered in tapping mode at a scan rate of 1 Hz. Nearly all SEM studies have been conducted with environmental FEI Quanta 450 scanning electron microscope in high vacuum mode. Unconjugated monodispersed 50 nm gold colloids (Tedd Pella) were used as test media and drop-casted onto the back of the membrane before the sealing of the E-cell.

Acknowledgment. Authors thank Mr. C. Watts, Ms. H.D. Gates, Prof. J. Bozzola, and Prof. S. Aouadi (SIUC) for their help in preparation of the experiment, equipment, and SEM imaging. The SIUC part of the research was supported through NSF ECCS-0925837 grant. J.H. thanks NSF for a CAREER award (DMR-0955612) and the Alfred P. Sloan Research Foundation for a Fellowship.

REFERENCES AND NOTES

1. Abrams, I.; McBain, J. A Closed Cell for Electron Microscopy. *J. Appl. Phys.* **1944**, *15*, 607–609.
2. Swift, J.; Brown, A. An Evironmental Cell for the Examination of Wet Biological Specimens at Atmospheric Pressure by Transmission Scanning Electron Microscopy. *J. Phys. E* **1970**, *3*, 924.
3. Parsons, D.; Matricardi, V.; Moretz, R.; Turner, J. Electron Microscopy and Diffraction of Wet Unstained and Unfixed Biological Objects. *Adv. Biol. Med. Phys.* **1974**, *15*, 161.
4. Boyes, E. D.; Gai, P. L. Environmental High Resolution Electron Microscopy and Applications to Chemical Science. *Ultramicroscopy* **1997**, *67*, 219–232.

5. Sharma, R.; Weiss, K. Development of a TEM To Study *In Situ* Structural and Chemical Changes at an Atomic Level Dduring Gas−Solid Interactions at Elevated Temperatures. *Microsc. Res. Tech.* **1998**, *42*, 270–280.
6. Daulton, T. L.; Little, B. J.; Lowe, K.; Jones-Meehan, J. *In Situ* Environmental Cell-Transmission Electron Microscopy Study of Microbial Reduction of Chromium(VI) Using Electron Energy Loss Spectroscopy. *Microsc. Microanal.* **2001**, *7*, 470–485.
7. Gai, P. L. Developments in *In Situ* Environmental Cell High-Resolution Electron Microscopy and Applications to Catalysis. *Top. Catal.* **2002**, *21*, 161–173.
8. Thiberge, S.; Zik, O.; Moses, E. An Apparatus for Imaging Liquids Cells, and Other Wet Samples in the Scanning Electron Microscopy. *Rev. Sci. Instrum.* **2004**, *75*, 2280–2289.
9. Cohen, O.; Beery, R.; Levit, S.; Ilany, J.; Schwartz, I.; Shabtai, M.; Anaby, D.; Cohen, D.; Alfici, R.; Czerniak, A.; *et al.* Scanning Electron Microscopy of Thyroid Cells under Fully Hydrated Conditions-A Novel Technique for a Seasoned Procedure: A Brief Observation. *Thyroid* **2006**, *16*, 997–1001.
10. Radisic, A.; Ross, F. M.; Searson, P. C. *In Situ* Study of the Growth Kinetics of Individual Island Electrodeposition of Copper. *J. Phys. Chem. B* **2006**, *110*, 7862–7868.
11. Jonge, N.; Peckys, D. B.; Kremers, G.; Piston, D. Electron Microscopy of Whole Cells in Liquid with Nanometer Resolution. *Proc. Natl. Acad. Sci. U.S.A.* **2009**, *106*, 2159.
12. Grogan, J. M.; Bau, H. H. The Nanoaquarium: A Platform for *In Situ* Transmission Electron Microscopy in Liquid Media. *J. Microelectromech. Syst.* **2010**, *19*, 885–894.
13. Kolmakova, N.; Kolmakov, A. Scanning Electron Microscopy for *In Situ* Monitoring of Semiconductor−Liquid Interfacial Processes: Electron Assisted Reduction of Ag Ions from Aqueous Solution on the Surface of TiO_2 Rutile Nanowire. *J. Phys. Chem. C* **2010**, *114*, 17233–17237.
14. See: http://www.quantomix.com; http://www.2spi.com; http://www.protochips.com.
15. Novoselov, K. S.; Jiang, D.; Schedin, F.; Booth, T. J.; Khotkevich, V. V.; Morozov, S. V.; Geim, A. K. Two-Dimensional Atomic Crystals. *Proc. Natl. Acad. Sci. U.S.A.* **2005**, *102*, 10451–10453.
16. Pacile, D.; Meyer, J. C.; Girit, C. O.; Zettl, A. The Two-Dimensional Phase of Boron Nitride: Few-Atomic-Layer Sheets and Suspended Membranes. *Appl. Phys. Lett.* **2008**, 92.
17. Hernandez, Y.; Nicolosi, V.; Lotya, M.; Blighe, F. M.; Sun, Z. Y.; De, S.; McGovern, I. T.; Holland, B.; Byrne, M.; Gun'ko, Y. K.; *et al.* High-Yield Production of Graphene by Liquid-Phase Exfoliation of Graphite. *Nat. Nanotechnol.* **2008**, *3*, 563–568.
18. Emtsev, K. V.; Bostwick, A.; Horn, K.; Jobst, J.; Kellogg, G. L.; Ley, L.; McChesney, J. L.; Ohta, T.; Reshanov, S. A.; Rohrl, J.; *et al.* Towards Wafer-Size Graphene Layers by Atmospheric Pressure Graphitization of Silicon Carbide. *Nat. Mater.* **2009**, *8*, 203–207.
19. Kim, K. S.; Zhao, Y.; Jang, H.; Lee, S. Y.; Kim, J. M.; Ahn, J. H.; Kim, P.; Choi, J. Y.; Hong, B. H. Large-Scale Pattern Growth of Graphene Films for Stretchable Transparent Electrodes. *Nature* **2009**, *457*, 706–710.
20. Stankovich, S.; Dikin, D. A.; Piner, R. D.; Kohlhaas, K. A.; Kleinhammes, A.; Jia, Y.; Wu, Y.; Nguyen, S. T.; Ruoff, R. S. Synthesis of Graphene-Based Nanosheets *via* Chemical Reduction of Exfoliated Graphite Oxide. *Carbon* **2007**, *45*, 1558–1565.
21. Turchanin, A.; Beyer, A.; Nottbohm, C. T.; Zhang, X.; Stosch, R.; Sologubenko, A.; Mayer, J.; Hinze, P.; Weimann, T.; Gölzhäuser, A. One Nanometer Thin Carbon Nanosheets with Tunable Conductivity and Stiffness. *Adv. Mater.* **2009**, *21*, 1233–1237.
22. Aleman, B.; Regan, W.; Aloni, S.; Altoe, V.; Alem, N.; Girit, C.; Geng, B. S.; Maserati, L.; Crommie, M.; Wang, F.; *et al.* Transfer-Free Batch Fabrication of Large-Area Suspended Graphene Membranes. *ACS Nano* **2010**, *4*, 4762–4768.
23. Meyer, J. C.; Girit, C. O.; Crommie, M. F.; Zettl, A. Imaging and Dynamics of Light Atoms and Molecules on Graphene. *Nature* **2008**, *454*, 319–322.
24. Wilson, N. R.; Pandey, P. A.; Beanland, R.; Young, R. J.; Kinloch, I. A.; Gong, L.; Liu, Z.; Suenaga, K.; Rourke, J. P.; York, S. J.; *et al.* Graphene Oxide: Structural Analysis and Application as a Highly Transparent Support for Electron Microscopy. *ACS Nano* **2009**, *3*, 2547–2556.
25. Bunch, J. S.; Verbridge, S. S.; Alden, J. S.; van der Zande, A. M.; Parpia, J. M.; Craighead, H. G.; McEuen, P. L. Impermeable Atomic Membranes from Graphene Sheets. *Nano Lett.* **2008**, *8*, 2458–2462.
26. Booth, T. J.; Blake, P.; Nair, R. R.; Jiang, D.; Hill, E. W.; Bangert, U.; Bleloch, A.; Gass, M.; Novoselov, K. S.; Katsnelson, M. I.; *et al.* Macroscopic Graphene Membranes and Their Extraordinary Stiffness. *Nano Lett.* **2008**, *8*, 2442–2446.
27. Stolyarova, E.; Stolyarov, D.; Bolotin, K.; Ryu, S.; Liu, L.; Rim, K. T.; Klima, M.; Hybertsen, M.; Pogorelsky, I.; Pavlishin, I.; *et al.* Observation of Graphene Bubbles and Effective Mass Transport under Graphene Films. *Nano Lett.* **2009**, *9*, 332–337.
28. Dikin, D. A.; Stankovich, S.; Zimney, E. J.; Piner, R. D.; Dommett, G. H. B.; Evmenenko, G.; Nguyen, S. T.; Ruoff, R. S. Preparation and Characterization of Graphene Oxide Paper. *Nature* **2007**, *448*, 457–460.
29. Chen, C. M.; Yang, Q. H.; Yang, Y. G.; Lv, W.; Wen, Y. F.; Hou, P. X.; Wang, M. Z.; Cheng, H. M. Self-Assembled Free-Standing Graphite Oxide Membrane. *Adv. Mater.* **2009**, *21*, 3007.
30. Kolmakov, A.; Dikin, D.; Cote, L. J.; Huang, J.; Kazemian Abyaneh, M.; Amati, M.; Gregoratti, L.; Günther, S.; Kiskinova, M. Graphene Oxide Windows for *In Situ* Environmental Cell Photoelectron Spectroscopy. *Nat. Nanotechnol.* **2011**, *6*, 651–657.
31. Cote, L. J.; Kim, F.; Huang, J. X. Langmuir−Blodgett Assembly of Graphite Oxide Single Layers. *J. Am. Chem. Soc.* **2009**, *131*, 1043–1049.
32. Kim, J.; Cote, L. J.; Kim, F.; Yuan, W.; Shull, K. R.; Huang, J. Graphene Oxide Sheets at Interfaces. *J. Am. Chem. Soc.* **2010**, *132*, 8180–8186.
33. Kim, F.; Cote, L. J.; Huang, J. Graphene Oxide: Surface Activity and Two Dimensional Assembly. *Adv. Mater.* **2010**, *22*, 1954–1958.
34. Erickson, K.; Erni, R.; Lee, Z.; Alem, N.; Gannett, W.; Zettl, A. Determination of the Local Chemical Structure of Graphene Oxide and Reduced Graphene Oxide. *Adv. Mater.* **2010**, *22*, 4467–4472.
35. Gomez-Navarro, C.; Meyer, J. C.; Sundaram, R. S.; Chuvilin, A.; Kurasch, S.; Burghard, M.; Kern, K.; Kaiser, U. Atomic Structure of Reduced Graphene Oxide. *Nano Lett.* **2010**, *10*, 1144–1148.
36. Chen, C. M.; Yang, Q. H.; Yang, Y. G.; Lv, W.; Wen, Y. F.; Hou, P. X.; Wang, M. Z.; Cheng, H. M. Self-Assembled Free-Standing Graphite Oxide Membrane. *Adv. Mater.* **2009**, *21*, 3541–3541.
37. Yunker, P. J.; Still, T.; Lohr, M. A.; Yodh, A. G. Suppression of the Coffee-Ring Effect by Shape-Dependent Capillary Interactions. *Nature* **2011**, *476*, 308–311.
38. Beams, J. *Structure and Properties of Thin Films*; Wiley and Sons: New York, 1959; pp 183−192.
39. Small, M. K.; Nix, W. D. Analysis of the Accuracy of the Bulge Test in Determining the Mechanical Properties of Thin Films. *J. Mater. Res.* **1992**, *7*, 1553–1563.
40. Behar, V.; Nechushtan, A.; Kliger, Y.; Gileadi, O.; Sprinzak, D.; Zik, O.; Karni, Y. Methods for SEM Inspection of Fluid Containing Samples. U.S. Patent 7,230,242 B2, 2007.
41. Hummers, W. S.; Offeman, R. E. Preparation of Graphitic Oxide. *J. Am. Chem. Soc.* **1958**, *80*, 1339.
42. Goldstein, J. *Scanning Electron Microscopy and X-ray Microanalysis*; Springer: Berlin, 2003; Vol. 1.
43. Haase, F.; Detemple, P.; Schmitt, S.; Lendle, A.; Haverbeck, O.; Doll, T.; Gnieser, D.; Bosse, H.; Frase, G. Electron Permeable Membranes for MEMS Electron Sources. *Sens. Actuators, A* **2006**, *132*, 98–103.
44. Pacilé, D.; Meyer, J. C.; Fraile Rodriguez, A.; Papagno, M.; Gomez-Navarro, C.; Sundaram, R. S.; Burghard, M.; Kern, K.; Carbone, C.; Kaiser, U. Electronic Properties and Atomic Structure of Graphene Oxide Membranes. *Carbon* **2011**, *44*, 966–972.